International Journal of Applied Earth Observation and Geoinformation 152 (2026) 105444

Contents lists available at ScienceDirect

International Journal of Applied Earth Observation and Geoinformation

journal homepage: www.elsevier.com/locate/jag

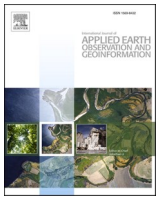

Quantifying changes in annual lichen volume for woodland caribou in Newfoundland using Landsat time series

Catherine Beaulieu [a,*], Nicholas C. Coops [b], Alexandre Morin-Bernard [a], Steeve D. Côté [c], Alexis Achim [a]

[a] Faculté de foresterie, de géographie et de géomatique, Université Laval, 2425 rue de la Terrasse, Québec, QC G1V 0A6, Canada
[b] Faculty of Forestry, University of British Columbia, 2424 Main Mall, Vancouver, BC V6T 1Z4, Canada
[c] Département de biologie and Centre d'études nordiques, Université Laval, 1045, avenue de la Médecine, Québec, QC G1V 0A6, Canada

ARTICLE INFO

Keywords:
Lichen volume
Boreal caribou conservation
Landsat
Remote sensing
Boreal forest
Newfoundland

ABSTRACT

Terrestrial and arboreal lichen are the primary winter food source of the threatened boreal ecotype of woodland caribou (*Rangifer tarandus caribou*). Despite its essential role, lichen biomass, a key factor of caribou habitat suitability, remains poorly quantified in forested landscapes, limiting effective habitat management and recovery planning. Our objective was to estimate lichen volume across two Newfoundland (Canada) boreal caribou herd ranges (Gros Morne and Gaff Topsails) using vegetation-specific models that integrate 1984–2022 Landsat Best Available Pixel composites with annual vegetation classifications from the National Terrestrial Ecosystem Monitoring System. Field data from 66 plots informed zero-inflated gamma models for coniferous forests, wetlands, barren land and shrublands. Predictors included spectral reflectance, vegetation indices, and vegetation type interactions. Model predictions closely matched observed lichen volume (pooled $R^2 = 0.77$, RMSE = 8.58 $dm^3\ m^{-2}$). Spatial outputs revealed widespread low lichen volume, with the highest volume in coniferous forests. Temporal trends showed a general increase in lichen volume since the early 1990s, with faster recovery across Gros Morne—potentially aided by the protected national park—compared to the more disturbed Gaff Topsails, where historical disturbances could have slowed early recovery. Estimated lichen biomass showed that patches reaching ~3000 $kg{\cdot}ha^{-1}$—a level typical of stands preferentially used by caribou in winter—were rare but widely distributed across the landscape. These vegetation-stratified, long-term estimates of lichen volume provide a key tool for assessing habitat suitability and guiding conservation strategies aimed at supporting woodland caribou recovery across Newfoundland.

1. Introduction

Most caribou and reindeer (*Rangifer tarandus*) populations worldwide have declined for the last two to four decades, although the drivers vary by ecotype (Festa-Bianchet et al., 2011; COSEWIC, 2014). For boreal caribou, human-induced habitat changes—particularly timber harvesting—have reduced access to mature forest habitat and increased predation risk through the expansion of early seral vegetation, benefiting alternate prey such as moose *(Alces alces*), which in turn supports higher predator populations (Wittmer et al., 2007; Anderson et al., 2018). This ecological shift leads to a phenomenon known as apparent competition, wherein predators sustained by abundant prey, such as moose, also prey upon caribou, further driving their decline (Christopherson et al., 2019). Compounding these effects, the widespread loss of old-growth forests driven primarily by timber harvesting has further accelerated caribou population declines by diminishing lichen-rich winter habitat, a critical resource that can take decades to recover (Boucher et al., 2009; Cichowski et al., 2022; Waterhouse et al., 2011).

The boreal ecotype of caribou—inhabiting critical forest regions for forest management—is therefore listed as 'Threatened' under the Species at Risk Act (SARA) (Environment and Climate Change Canada, 2020). Despite a few ongoing conservation efforts, little progress has been made in reducing anthropogenic disturbances, and most populations continue to decline (Festa-Bianchet et al., 2011). Effective recovery planning requires maintaining suitable habitat, including spatial configuration and connectivity, at landscape scales (Courtois et al., 2008; O'Brien et al., 2006; Ruppert et al., 2016).

* Corresponding author.
E-mail address: catherine.beaulieu.14@ulaval.ca (C. Beaulieu).

https://doi.org/10.1016/j.jag.2026.105444
Received 22 January 2026; Received in revised form 30 March 2026; Accepted 23 June 2026
Available online 29 June 2026

Lichen availability is central to defining habitat suitability for caribou conservation, particularly during the critical winter season when caribou face trade-offs between forage abundance and accessibility (Bergerud, 1972; McMullin et al., 2011; Parker et al., 2005). Deep snow increases locomotion and foraging costs, with potential consequences for maternal condition and calf size the following spring (Adams, 2005). Quantifying lichen biomass is, therefore, crucial for developing effective conservation strategies (Courtois et al., 2004).

Lichen biomass, cover, and volume have been estimated using combinations of field sampling, remote sensing, and modelling approaches. Early remote sensing work focused on mapping *Cladonia* lichen cover using its unique spectral signatures, distinguishable from green vegetation by their absorption of ultraviolet and blue wavelengths (Fraser et al., 2022; He et al., 2021; Petzold and Goward, 1988; Théau et al., 2005). While lichen cover provides insight into habitat suitability (Rickbeil et al., 2017a), biomass is the most ecologically meaningful metric for caribou forage assessment (Johnson et al., 2001; Falldorf et al., 2014). Estimating biomass over large areas is challenging because it requires density and moisture data, which are difficult to assess remotely and require extensive field measurements (McMullin et al., 2011; Nelson et al., 2013). Consequently, lichen volume has often been used as a proxy for biomass, enabling spatially explicit mapping using remotely sensed data (Falldorf et al., 2014; Greuel et al., 2021). Falldorf et al. (2014) developed the Lichen Volume Estimator (LVE) using Landsat Thematic Mapper (TM) images and successfully estimated lichen volume on the Hardangervidda plateau, Norway. Their estimator is based on two Landsat-derived indices—the Normalized Difference Lichen Index (NDLI; Nordberg, 1998) and the Normalized Difference Moisture Index (NDMI; Wilson & Sader, 2002)—which exploit contrasts between near-infrared (Band 4) and shortwave-infrared (Band 5) reflectance. These contrasts are effective because lichens exhibit lower near-infrared and higher shortwave-infrared reflectance than vascular vegetation, which is characterized by a strong near-infrared plateau associated with internal leaf structure (Ager & Milton, 1987; Petzold & Goward, 1988; Rees et al., 2004; Macander et al., 2020; Kuusinen et al., 2020). Rickbeil et al. (2017b) subsequently applied the LVE across a 700,000 km^2 region of the Canadian Arctic and revealed notable changes in barren-ground caribou movement rates in response to lichen volume estimates, emphasizing its importance for caribou conservation. However, the method has only been applied in relatively homogeneous tundra landscapes (Falldorf et al., 2014; Rickbeil et al., 2017b), and its applicability to structurally complex or forested ecosystems remains untested.

Creating accurate lichen distribution maps remains a significant challenge due to the difficulty of consistently linking remotely sensed spectral reflectance to lichen cover, volume, or biomass (Nelson et al., 2013; Falldorf et al., 2014; Rickbeil et al., 2017b). Terricolous lichens typically occur in small, discontinuous mats and share spectral similarities with mosses, shrubs, and other low-lying vegetation, complicating their detection using satellite imagery (Petzold & Goward, 1988; Nelson et al., 2013; Macander et al., 2020). These challenges are compounded by variability across landscape types, as predictive models often perform inconsistently when transferred beyond their calibration environments (Nelson et al., 2013; Fraser et al., 2022; Macander et al., 2020). Mapping lichens in structurally complex boreal forests, such as those in Newfoundland, presents further difficulties because ground lichens are frequently obscured by dense canopy cover and shadows, limiting their detectability from remotely sensed data (Fraser et al., 2022). Additionally, landscape heterogeneity reduces the effectiveness of generalized models developed for more homogeneous tundra regions. For example, Macander et al. (2020) demonstrated that lichen models commonly overpredict in low-cover areas and underpredict in high-cover zones, particularly where lichen appears patchy or is hidden by canopy or shadow. Together, these limitations restrict the utility of coarse-resolution satellite models in forested ecosystems and highlight the need for more tailored, habitat-specific approaches that explicitly account for how different environments influence ground lichen availability—an aspect that has not yet been studied in detail in boreal forests.

Our objective was to produce accurate, spatially explicit lichen volume maps using open-access satellite data, tailored to the structurally diverse habitats of Newfoundland, Canada. To achieve this, we used the Best Available Pixel (BAP) Landsat composites from 1984 to 2022, which provide temporally consistent, cloud-free annual observations ideal for long-term monitoring (White et al., 2014). By integrating these composites with annual vegetation classifications, we aimed to capture how lichen availability varies across habitat types and through time. Rather than applying a single estimator across all environments likely to support ground lichen in Newfoundland, we developed a stratified modeling framework that reflects the ecological and structural variability within each vegetation class. We focused on the ranges of two boreal caribou herds—Gros Morne and Gaff Topsails—as representative areas for assessing lichen availability and habitat conditions across Newfoundland's boreal ecosystems, each shaped by distinct disturbance histories and vegetation structures.

2. Materials and methods

2.1. Study area and herd selection

Newfoundland is a 106,000 km^2 island off eastern Canada, home to approximately 30,000 boreal caribou distributed across 14 recognized subpopulations (Fisheries, Forestry and Agriculture, 2021; Mahoney et al., 2016). The island's cool maritime climate, shaped by the cold Labrador Current and the Gulf Stream, supports boreal forests where 95% of the total wood volume consists of balsam fir (*Abies balsamea* (L.) Mill), black spruce (*Picea mariana* (Mill.) B.S.P.), and white birch (*Betula papyrifera* Marsh.) (Meades & Roberts, 1992). These forests are part of the Boreal Shield ecozone, which spans across North America and covers approximately 552 million hectares (Arsenault et al., 2016; Matasci et al., 2018). Harvesting activities on the island have historically targeted mature conifer stands for pulp and paper production, primarily through clear-cutting since the 1920s (Mahoney & Virgl, 2003).

To assess the effects of forest harvesting on caribou habitat and lichen availability, we selected two study herds with comparable vegetation composition but contrasting disturbance histories. The Gros Morne herd occupies a largely intact landscape within Gros Morne National Park (northwestern polygon, Fig. 2). Its range lies mostly in the Long Range Barrens ecoregion—an extension of the Appalachian Range characterized by elevations of 600–700 m, wet boreal forest, and alpine heath (Manson et al., 2020; Meades, 2008)—and slightly overlaps the Northern Peninsula and Western Newfoundland forest ecoregions, all dominated by balsam fir (Meades, 2008). In contrast, the Gaff Topsails herd also inhabits a high plateau within the Long Range Barrens ecoregion, but in an area that has experienced extensive forest harvesting (southwestern polygon, Fig. 2). The landscape within this herd range is dominated by bogs, fens, and shrub barrens, with remnant patches of black spruce and balsam fir in sheltered valleys (Damman, 1983).

2.2. Modeling framework

2.2.1. Data acquisition

2.2.1.1. Landsat data and derived products. Landsat Best Available Pixel (BAP) composites (White et al., 2014) together with annual land cover maps from the National Terrestrial Ecosystem Monitoring System (NTEMS) (Hermosilla et al., 2018, 2022), from 1984 to 2022, served as the primary inputs for spectral and vegetation characterization across the study area.

The BAP approach generates annual cloud-free surface reflectance

2.2.1. Data acquisition

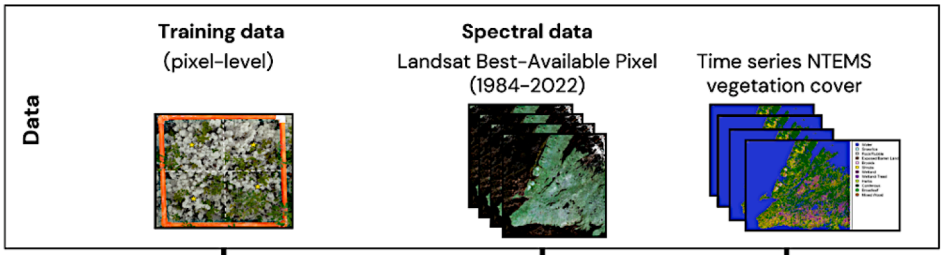

2.2.2. Modeling

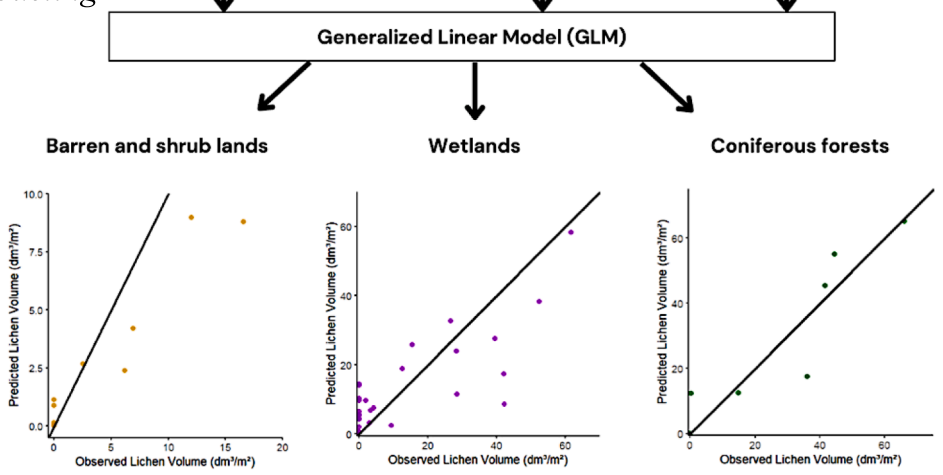

2.2.3. Application

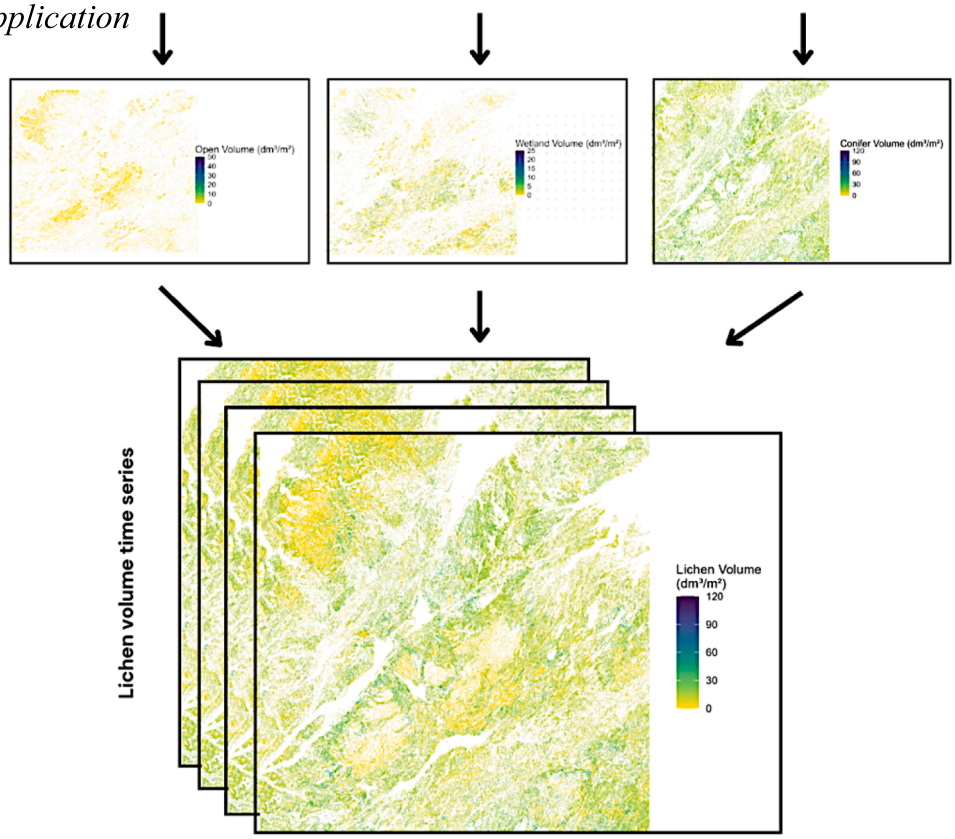

Fig. 1. Modeling framework for lichen volume estimation using field data, Landsat Best Available Pixel (BAP) composites, and National Terrestrial Ecosystem Monitoring System (NTEMS) land cover maps (1984–2022; see Sections 2.2.1–2.2.3 for details).

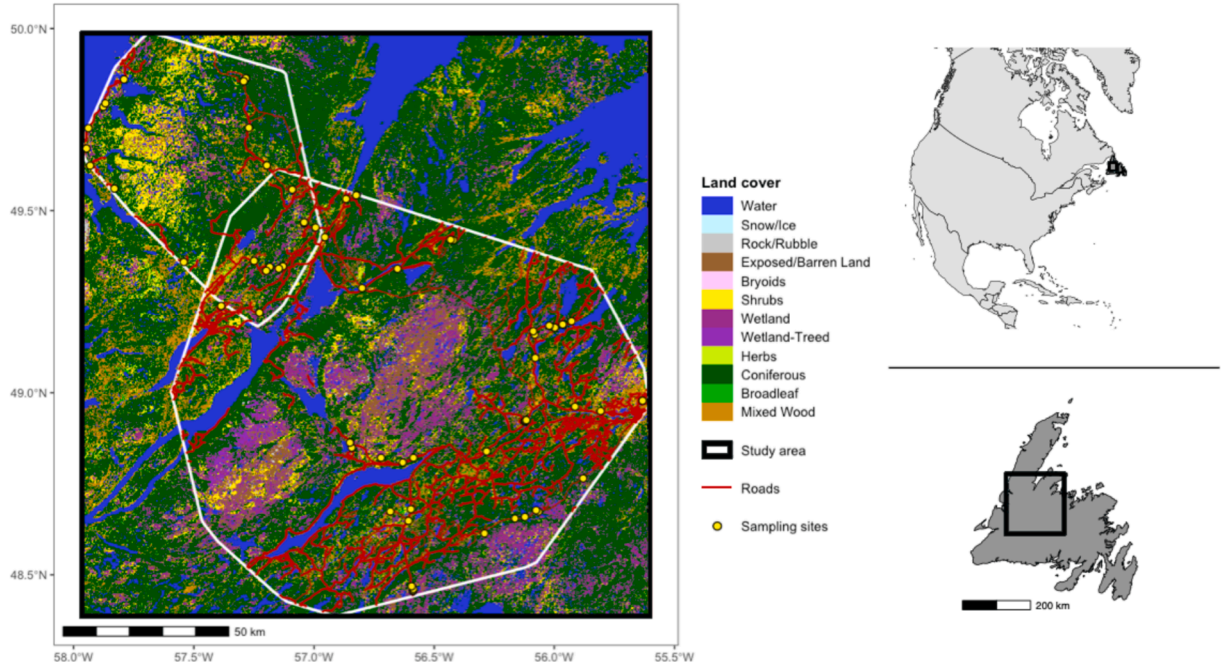

Fig. 2. Land cover classification from the National Terrestrial Ecosystem Monitoring System (NTEMS) dataset, with sampled sites (yellow points; n = 66) distributed within the Gros Morne (northwest) and Gaff Topsails (southeast) 97% Minimum Convex Polygons (MCPs). Roads are shown to indicate accessibility, as all sampled plots were located within 50–300 m of a road. The black outline delineates the study area over which lichen volume models were applied. Insets (right) show the location of this study area within North America (top) and within the island of Newfoundland (bottom).

composites at 30 m resolution by selecting the highest-scoring pixel from candidate Landsat-4, -5, -7, and -8 observations acquired between 1 July and 30 August, a period aligned with peak vegetation growth across Canadian forests (McKenney et al., 2006; White et al., 2014). Candidate scenes are retrieved from the USGS archive as Level-1 Terrain-Corrected (L1T) products and subsequently atmospherically corrected to surface reflectance prior to compositing (White et al., 2014). Pixel scoring functions rank candidate observations based on the acquisition sensor (i.e., penalizing Landsat 7 scenes due to the Scan Line Corrector (SLC) failure), target date, cloud/shadow proximity, and atmospheric opacity; the highest-scoring observation is then selected for each pixel location in the annual composite (Hermosilla et al., 2015; White et al., 2014).

NTEMS produces high-resolution (30 m) annual land cover maps of Canada's forested ecosystems from 1984 to 2022, using a combination of Landsat-based BAP composites, forest disturbance information, and ancillary data such as topography and hydrology (Hermosilla et al., 2018, 2022). Each NTEMS map distinguishes twelve primary land-cover classes representing forested and non-forested ecosystems: coniferous, broadleaf, mixedwood and wetland-treed forests; wetland; shrubs (hereafter referred to as shrubland in the text); herb; bryoid; exposed/barren land; rock/rubble; water; and snow/ice.

2.2.1.2. Field sampling. We initially applied the Lichen Volume Estimator (Falldorf et al., 2014) to the 2021 BAP composite—the most recent cloud-free imagery prior to fieldwork—to guide site selection. Although sampling occurred in August 2023, the slow growth rate of lichens (Nash, 2008) and the absence of intervening disturbances supported the use of 2021 imagery.

The LVE relies on two Landsat-derived spectral indices, NDLI and NDMI, which were computed from Landsat surface reflectance as follows:

$$NDLI = \frac{SWIR_1 - NIR}{SWIR_1 + NIR}$$

$$NDMI = \frac{NIR - SWIR_1}{NIR + SWIR_1}$$

where NIR corresponds to Landsat TM Band 4 and $SWIR_1$ to Band 5.

The LVE combines the NDLI and the NDMI within a two-dimensional Gaussian function:

$$LVE(NDLI, NDMI) = a \times e^{-0.5 \times \left(\left(\frac{NDLI - NDLI_{mean}}{b} \right)^2 + \left(\frac{NDMI - NDMI_{mean}}{c} \right)^2 \right)}$$

where NDLImean and NDMImean are the mean values of the NDLI and NDMI respectively, and a, b and c are the normal distribution parameters. The LVE was used as an exploratory tool to identify potential lichen-rich areas but was applied only to land cover types classified by the NTEMS land cover classification data (Hermosilla et al., 2018, 2022) as likely to support ground lichen, i.e. coniferous forests, mixed woods, wetlands, shrublands, and barrens.

However, field observations revealed that the LVE often underestimated lichen in closed-canopy areas, where satellite imagery fails to detect ground cover, and overestimated it in open barren land and some wetlands due to surface reflectance from disturbances such as roads, cutblocks, or exposed rock. To address these limitations, we visually interpreted high-resolution satellite imagery (Google Earth) to identify additional candidate plots with visible lichen cover across the same five NTEMS-defined vegetation types. This combined approach ensured that our sampling design captured the full gradient of lichen abundance across all relevant land cover classes.

A total of 66 field sites were sampled during August 2023 (Appendix A, Table A1), all randomly distributed within the 97% Minimum Convex Polygon (MCP) constructed from GPS collar data provided by Natural Resources Canada (NRCan) (Fig. 2). The MCPs were derived from GPS-collar telemetry for 23 adult Gros Morne caribou (2011–2018) and 35 Gaff Topsails caribou (2005–2018), with locations recorded at ~2-hour intervals across all major caribou seasons. The use of a 97% MCP—rather than the more conservative 95%—allowed us to include areas reflecting occasional movements by the Gaff Topsails caribou

herd, while maintaining logistical feasibility for the field crew. All sampled plots were located within 50 to 300 m of a road to ensure accessibility. Due to discrepancies between mapped and observed vegetation types, or limited accessibility (particularly in barren lands), some vegetation types included fewer than five sampled sites per region.

At each sampled site, a 500 m^2 circular plot (radius ≈ 12.6 m) was established, within which 11 microplots were arranged along a central north–south transect and two parallel transects located 6 m to the east and west, with microplots spaced 5 m apart along each transect (Appendix B, Fig. B1). Microplots consisted of 50 × 50 cm polyvinyl chloride (PVC) quadrats, visually divided into four sections to aid cover estimation. Lichen height was measured to the nearest centimeter at the approximate center of each microplot, and cover was visually estimated in 10% increments. If no lichen was present in the plot, only the central microplot was assessed. Lichen volume (dm^3/m^2) was calculated as:

$$LichenVolume\left(\frac{dm^3}{m^2}\right) = \frac{Lichenheight(dm)xplotarea\left(dm^2\right)xLichencover(\%)}{plotarea(m^2)}$$

where lichen height is converted to decimeters, and the plot area refers to that of the microplot (0.25 m^2 or 25 dm^2). Microplot locations were recorded using a high-precision Trimble R2 GPS unit, enabling post hoc verification of satellite-derived vegetation types and lichen categories. Basic forest characteristics were also recorded at each site for five merchantable trees and noting their species and canopy dominance class (dominant, co-dominant, or intermediate) to verify vegetation type classifications derived from the NTEMS land cover data. In addition, a standardized photo set (downward and cardinal orientations) was collected for quality assurance. These field measurements served as the basis for subsequent model development (Section 2.2.2).

2.2.2. Modeling

The 66 sampled field sites were used as training data to develop predictive models of lichen volume. For each site, lichen volume (dm^3 m^{-2}) was derived from microplot measurements: when lichen was present, volume values from the 11 microplots were averaged, whereas plots without lichen contained only a single assessed microplot. This aggregation to the plot scale ensured consistency with the 30 m spatial resolution of Landsat imagery, for which only one reflectance value is available per plot. Reflectance values from all Landsat bands were extracted at each plot centroid from the 2021 BAP composite, and a suite of vegetation indices commonly used to characterize greenness, moisture, and disturbance were computed from these reflectance values.

To account for structural and spectral differences across land cover types—because distinct cover types exhibit different canopy structures and spectral responses that influence the detectability of ground lichens— we developed separate models for coniferous forests, wetlands, and open lands (i.e. barren land and shrubland), as defined by the NTEMS land cover classification (Hermosilla et al., 2018, 2022; see Section 2.3.1). Exploratory plots suggested that barren and shrubland sites may respond differently to moisture-sensitive indices such as NDWI, with lichen volume showing opposite tendencies between the two cover types (Appendix C, Fig. C5). To accommodate these potential differences while avoiding overfitting, and given their similar ecological structure (short vegetation and minimal canopy cover), we modeled barren and shrubland sites jointly, including vegetation type as an interaction term with the spectral predictors. Mixed wood forests were excluded from model development because field data confirmed the near absence of terrestrial lichens in those areas; accordingly, these pixels were assigned a lichen volume of zero during spatial prediction.

For each class, lichen volume was modeled using zero-inflated gamma models (ziGamma) implemented in the *glmmTMB* package (Brooks et al., 2017) in R version 4.4.2 (R Core Team, 2024), an approach well suited to datasets with a high frequency of zeros. A binary variable distinguishing zero from non-zero lichen volume was created to support the zero-inflation component. Multiple models were fitted and compared using ecologically relevant spectral predictors derived from the 2021 Landsat BAP composite—the closest cloud-free imagery to the 2023 field data at the time this part of the analysis was performed.

Predictor variables were first screened using exploratory scatterplots to identify spectral variables showing potential relationships with observed lichen volume, and correlation matrices to identify redundant predictors and avoid multicollinearity among spectral bands and vegetation indices (Appendix C). This screening step was used to define a subset of predictors for model development. Variables showing a plausible relationship with lichen volume were retained for model development, while predictors that were correlated were not included together within the same candidate model to limit multicollinearity. Using this subset of predictors, candidate models were developed for each vegetation class using combinations of surface reflectance bands (blue, green, red, SWIR1: Short-Wave Infrared Band 1) and vegetation indices representing greenness (NDVI: Normalized Difference Vegetation Index), moisture conditions (NDWI: Normalized Difference Water Index; TCW: Tasseled Cap Wetness), substrate brightness (TCB: Tasseled Cap Brightness), and disturbance or dryness (NBR: Normalized Burn Ratio) (Appendix D, Table D1).

Model selection was conducted using a sequential procedure. Specifically, (i) residual diagnostics were first assessed for all candidate models using the DHARMa package (Hartig, 2024), and models showing clear violations of model assumptions (e.g., strong deviations in QQ-plots, dispersion issues, or outliers) were excluded; (ii) the remaining models were then ranked using Akaike Information Criterion corrected for small sample size (AICc), and the three models with the lowest AICc values were retained; (iii) among these models, predictive performance was evaluated using root mean square error (RMSE) and prediction bias (mean signed prediction error), and models minimizing both metrics were preferred. Finally, Pseudo-R^2 was used as a complementary indicator of model fit. Models showing poor predictive performance (e.g., low pseudo-R^2 or inconsistent fit relative to observed data) were not retained, even when supported by AICc or residual diagnostics. Due to the limited number of field observations and the high correlation among several spectral bands, we opted for relatively simple zero-inflated Gamma models for each vegetation type (Table 1).

2.2.3. Model application

Annual lichen volume predictions were generated across the study area by applying the selected models to the full time series of Landsat Best Available Pixel (BAP) composites from 1984 to 2022 (White et al., 2014). The models were calibrated using the 2021 BAP composite, while the 2022 composite became available prior to the model application step and was therefore included in the prediction time series. For each year, the corresponding NTEMS land cover map was used to assign pixels to one of the three vegetation types (coniferous forests, wetlands, or open lands). The appropriate model was then applied to each pixel within its class, generating annual predictions of lichen volume at 30 m resolution across the study area. Model outputs were subsequently summarized and interpreted within the 97% Minimum Convex Polygons (MCPs) encompassing the Gros Morne and Gaff Topsails caribou herds.

To smooth interannual variability, account for residual cloud-related artefacts, and highlight long-term dynamics, a 7-year moving average was applied to the annual predictions. We tested several window sizes: shorter windows (3–5 years) retained visible artefacts, whereas longer windows (10 years) over-smoothed the data and masked ecological trends.

In addition, predicted lichen volume (dm^3 m^{-2}) was converted to biomass (kg ha^{-1}) to facilitate comparison with thresholds relevant to caribou winter forage. Bulk density was derived by combining Newfoundland lichen mat height measurements (0–14 cm, mean 3.8 cm) with published ground-lichen biomass values from boreal and coniferous forests (90–850 g m^{-2}; Edmonds & Bloomfield, 1984; Scotter, 1965; Arseneault et al., 1997; McMullin et al., 2011; Väre et al., 1996). Dividing these biomass values by mean mat height yielded a bulk-

Table 1
Candidate zero-inflated Gamma models for each vegetation type, with conditional formulas modelling positive lichen volume and zero-inflation formulas modelling structural zeros. Model performance was compared using the Akaike Information Criterion (AICc), pseudo-R^2, root mean square error (RMSE), and mean prediction bias. Bold rows indicate the selected model for each vegetation type.

Vegetation type	Model name	Conditional formula	Zero-inflation formula	AICc	Pseudo R^2	RMSE (dm^3/m^2)	Bias (dm^3/m^2)
Open Lands	Open1	`Volume_mean ~ NDVI`	`~ blue`	54.53	−4.20	11.51	6.36
	Open2	**`Volume_mean ~ NDWI * vegtype`**	**`~ NDWI`**	**57.64**	**0.75**	**2.50**	**−1.00**
	Open3	`Volume_mean ~ NDWI * vegtype`	`~ blue`	58.66	0.74	2.56	−1.04
Wetlands	**Wet1**	**`Volume_mean ~ green`**	**`~ TCW + green`**	**163.14**	**0.63**	**11.36**	**−0.08**
	Wet2	`Volume_mean ~ green + TCW`	`~ NBR + green`	165.01	0.54	12.72	0.50
	Wet3	`Volume_mean ~ green + NBR`	`~ TCW + green`	165.38	0.63	11.33	0.18
Coniferous	**Conf1**	**`Volume_mean ~ green`**	**`~ swir1`**	**69.86**	**0.91**	**6.42**	**0.32**
	Conf2	`Volume_mean ~ TCB`	`~ swir1`	70.37	0.84	8.66	0.51
	Conf3	`Volume_mean ~ red + nir`	`~ swir1`	99.09	0.59	13.75	2.4

density range of ca. 2.4–22.4 kg m^{-3}, which was multiplied by modeled volume to obtain biomass equivalents.

Finally, to better understand the drivers of temporal change, we examined how spatial and temporal patterns of predicted lichen volume related to vegetation structure and disturbance history. Specifically, we evaluated (i) how mean lichen volume changed over time within each vegetation type, (ii) how total lichen volume, calculated as the sum of all lichen volume values across all pixels and vegetation types and normalized by herd range area, changed over time, and (iii) whether areas exhibiting long-term volume loss corresponded to mapped disturbances. For the latter, we identified pixels experiencing net lichen volume loss between the first (1984–1988) and last (2018–2022) five-year periods of the time series and linked these pixels to disturbance attributes from the NTEMS change-type and change-year datasets. These datasets identify disturbance events annually using Landsat time-series through the Composite2Change (C2C) algorithm (White et al., 2017). The C2C framework produces annual, gap-free 30 m surface reflectance composites through best-available-pixel selection, cloud/shadow masking, temporal noise removal, and breakpoint detection (Hermosilla et al., 2015; Hermosilla et al., 2016). Disturbance events are classified in the NTEMS disturbance layer as wildfire, harvesting, road, or non–stand-replacing change (e.g., insects, disease, water stress). For our analyses, road and non–stand-replacing changes were grouped into a single "others" disturbance category to distinguish them from the major stand-replacing disturbances—fire and harvesting— which are the dominant drivers of land cover change in Newfoundland.

3. Results

The final zero-inflated gamma models selected for each vegetation class captured the key spectral–lichen relationships while remaining simple and interpretable, as reflected by model performance metrics including pseudo-R^2, RMSE, and bias (Table 1).

For open lands, the chosen model, *Open2*, included NDWI and its interaction with vegetation subtype, with NDWI predicting zero inflation. This model achieved the best overall fit (pseudo-R^2 = 0.75; RMSE = 2.5 dm^3/m^2; bias = –1.0 dm^3/m^2), outperforming the similar candidate model *Open3*. Although Open1 had the lowest AICc, it showed poor predictive performance, with a negative pseudo-R^2 and substantially higher RMSE and bias. Consequently, Open2 was retained as the most reliable model for predicting lichen volume in open lands.

In wetlands, model *Wet1* provided the best combination of fit and parsimony, using green reflectance in the conditional component and TCW and green in the zero-inflation component (pseudo-R^2 = 0.63; RMSE = 11.36 dm^3/m^2; bias = –0.08 dm^3/m^2). Adding predictors in *Wet2* and *Wet3* did not improve performance.

For coniferous forests, *Conf1*, which relied on green reflectance conditionally and SWIR1 for zero inflation, showed the lowest AICc and best fit (pseudo-R^2 = 0.91, RMSE = 6.42 $dm^3\ m^{-2}$, bias = 0.32 $dm^3\ m^{-2}$) and outperformed *Conf2* and *Conf3*.

Across open lands (shrublands and barrens), wetlands, and coniferous forests, the models generally captured the expected trends between spectral indices and lichen volume, with predicted values closely matching observations (Fig. 3). In open lands, predicted lichen volume exhibited a vegetation-specific curved response to NDWI: in shrublands (filled points), values remained near zero at low NDWI and began increasing only at intermediate values (~–0.70 to –0.67), whereas in barrens (hollow points) volume peaked beyond –0.67 and declined toward –0.60. In wetlands and coniferous forests, both predicted and observed lichen volume remained near zero at low green reflectance and then increased approximately linearly at higher values. Moisture-sensitive indices (TCW for wetlands; SWIR1 for conifers) were included in the zero-inflation component. When pooled across vegetation types, model agreement with observations was strong (pseudo-R^2 = 0.77, RMSE = 8.58 $dm^3\ m^{-2}$, bias = –0.22 $dm^3\ m^{-2}$), indicating consistent lichen–reflectance relationships across habitat types.

The modeling framework generated annual lichen volume maps at 30-m resolution for each vegetation type from 1984 to 2022 (see Appendix E, Fig. E1, for the 2022 map). Predicted volume ranged from 0 to ~120 $dm^3\ m^{-2}$, but most of the landscape supported low values: 95% of pixels were ≤21.2 $dm^3\ m^{-2}$, indicating that high-volume lichen patches are relatively rare yet widespread. Near-zero values were common—particularly in open lands and recently disturbed areas—where more than half of pixels were close to zero. When converted to biomass using the density estimate range (Section 2.2.3), the 95th percentile volume (21.2 dm^3/m^2) corresponds to ca 510–4700 $kg{\cdot}ha^{-1}$. Using the midpoint of this density range (~12 kg m^{-3}) provides a representative estimate of ~2540 kg ha^{-1}.

Mean lichen volume was consistently highest in coniferous forests, ranging between approximately 5.6 and 9.0 dm^3 per m^2 throughout the study period (Fig. 4). In contrast, wetlands and open lands supported much lower volumes, ranging between 1.0–1.3 $dm^3\ m^{-2}$ and 0.4–0.9 $dm^3\ m^{-2}$, respectively. While lichen volume remained relatively stable in wetlands and open lands throughout the time series, coniferous forests showed a general upward trend following an initial period of decline from 1987 to 1993.

As shown in Fig. 5, total lichen volume increased in both regions over the study period. In Gros Morne, the increase was more pronounced, particularly after the early 1990s following a period of decline between 1984 and 1993. The Gaff Topsails region exhibited a similar trajectory, but with a slower and more gradual recovery.

While some correspondence was observed between disturbance locations and areas of lichen volume loss, the relationship was not systematic. In Gaff Topsails, disturbances—primarily harvesting and fires—were more numerous and widespread, and overall volume gains were present but were less substantial compared to Gros Morne. The latter showed a general increasing trend in lichen volume across the study period (Fig. 5); however, Fig. 6 reveals the presence of localized declines. These declines were most pronounced outside the national park boundary, where a greater number of pixels exhibited net loss (red), particularly in the southwestern portion of the Gros Morne herd affected by past harvesting; no harvesting takes place within the park.

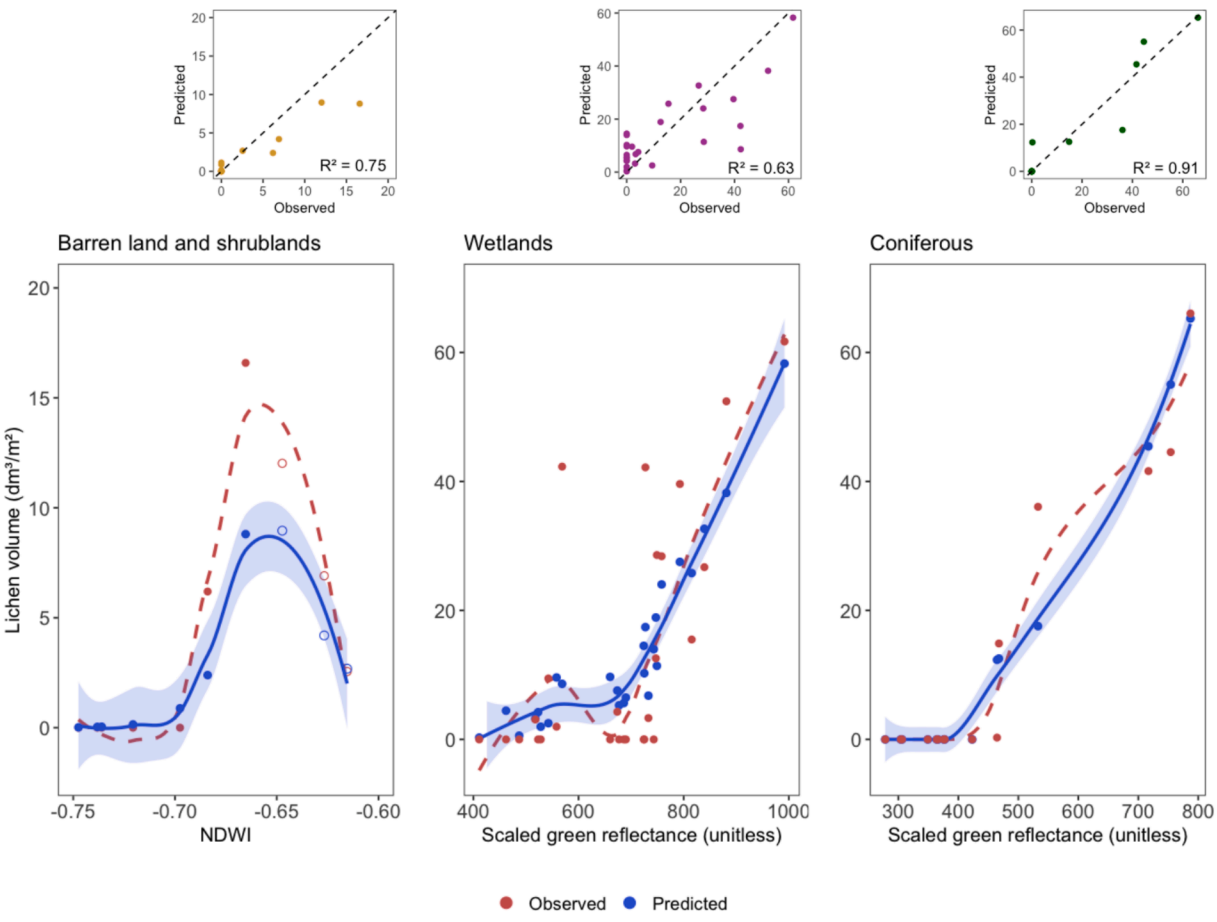

Fig. 3. Predicted (in blue) vs. observed (in red) lichen volume for each vegetation class in Newfoundland, Canada, based on the 66 field plots used for model calibration. Dashed red line shows the trend of observed lichen volume, added for visual comparison with model predictions (solid blue line). In the barren land and shrubland plot, hollow symbols represent barren sites and filled symbols represent shrublands. Small plots positioned above and to the right of each plot show predicted versus observed values of lichen volume for the same vegetation class as the panel directly below, with dashed 1:1 lines and R^2 values.

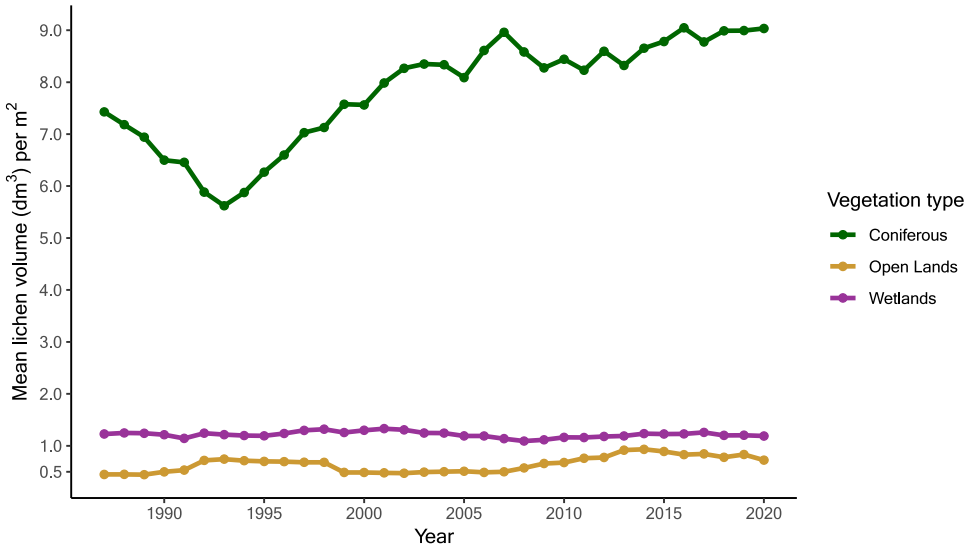

Fig. 4. Seven-year moving average of mean lichen volume (dm^3) per m^2 across three vegetation types: coniferous forests, wetlands, and open lands in our study area. The lines represent smoothed trends over time, where each point reflects the average lichen volume across a centered seven-year period and where each color represents a vegetation type.

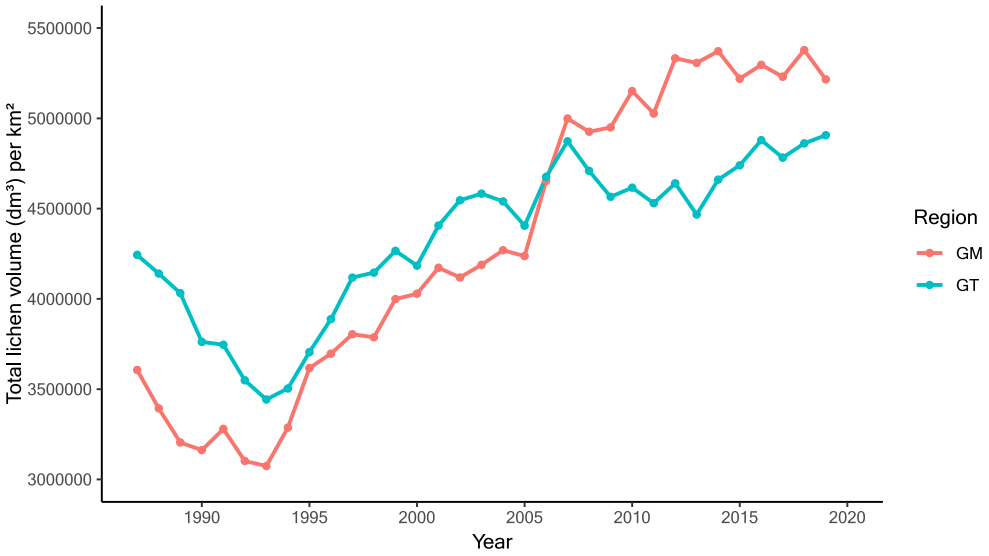

Fig. 5. Seven-year moving average of total lichen volume (dm^3 per km^2) for the Gros Morne (GM, red) and Gaff Topsails (GT, blue) caribou herd ranges. Annual lichen volume was summed across all 30-m pixels and divided by each region's area (km2), yielding a region-normalized measure of total lichen availability.

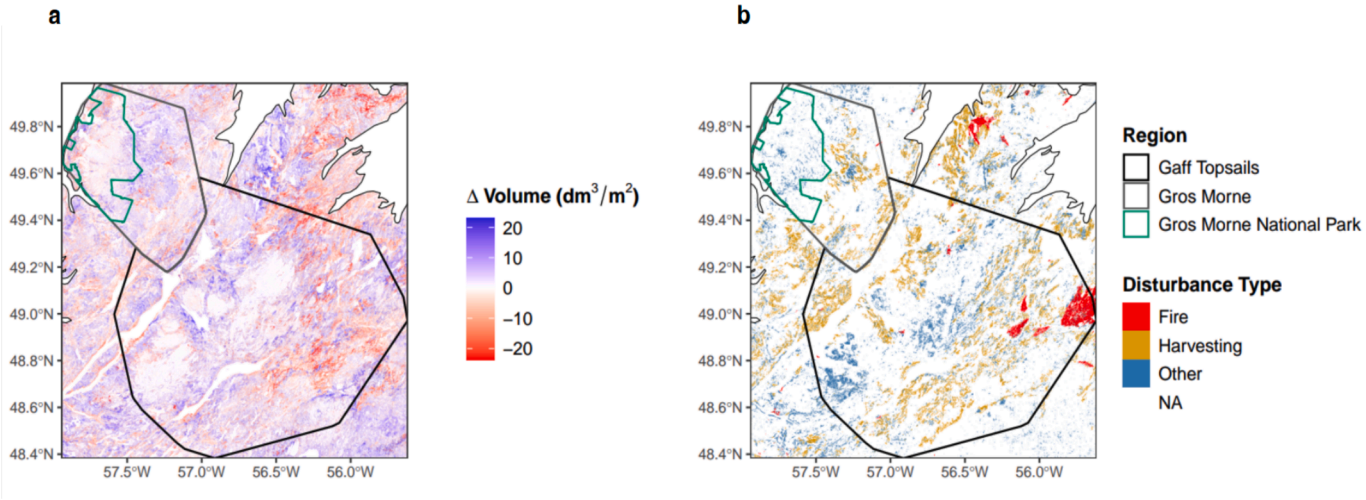

Fig. 6. (a) Net lichen volume change (dm^3/m^2) between 1984–1988 and 2018–2022 in our study area, where blue indicates gains and red indicates losses. (b) Spatial distribution of disturbances from the NTEMS change-type dataset (1984–2022), classified as fire, harvesting, and other disturbances (i.e. roads and non–stand-replacing changes such as insects, disease, or water stress). The 97% Minimum Convex Polygon (MCP) boundaries of the Gaff Topsails and Gros Morne caribou herd ranges are shown in black and grey, respectively; Gros Morne National Park is outlined in green.

Some years showed substantial lichen volume loss without a clear link to mapped disturbances (Fig. 6), as the spatial distribution of these losses did not clearly overlap with disturbance events. In the Gaff Topsails region, 15.5% of pixels exhibiting net lichen volume loss were directly associated with mapped disturbances, whereas this proportion was 8.9% in Gros Morne. When considering pixels located within 500 m of a disturbance —a distance consistent with the buffering approach used in boreal caribou disturbance assessments (Environment Canada, 2011)—this proportion increased to 58.9% in Gaff Topsails and 45.4% in Gros Morne, indicating that a substantial portion of lichen loss occurs in areas surrounding mapped disturbance pixels rather than within the disturbed pixels themselves.

Fig. 7 summarizes the disturbance types associated with pixels that showed net lichen loss over the study period. This analysis revealed that, while an early fire event in 1986 accounted for much of the initial loss in Gaff Topsails, harvesting increasingly became the dominant disturbance linked to lichen volume losses in more recent decades. In Gros Morne, where fire is rare, losses were more spatially localized and less systematically connected to mapped disturbance events. Since 2010, harvesting has emerged as the main disturbance associated with lichen volume loss in both regions, though in Gros Morne such activity occurs exclusively outside the park boundary, where harvesting is permitted (Fig. 6b).

4. Discussion

Our results demonstrate that vegetation-stratified models can reliably generate accurate, spatially explicit, long-term estimates of terrestrial lichen volume across Newfoundland's heterogeneous habitat types. Beyond producing four decades of high-resolution maps, the modelled time series reveals important ecological patterns: lichen volume generally increased after the early 1990s despite relatively high disturbance rates, with evidence of both localized declines and gains, but an overall positive balance. It also highlights contrasting regional dynamics between Gros Morne and Gaff Topsails, as well as the complex relationships between disturbance history and changes in lichen

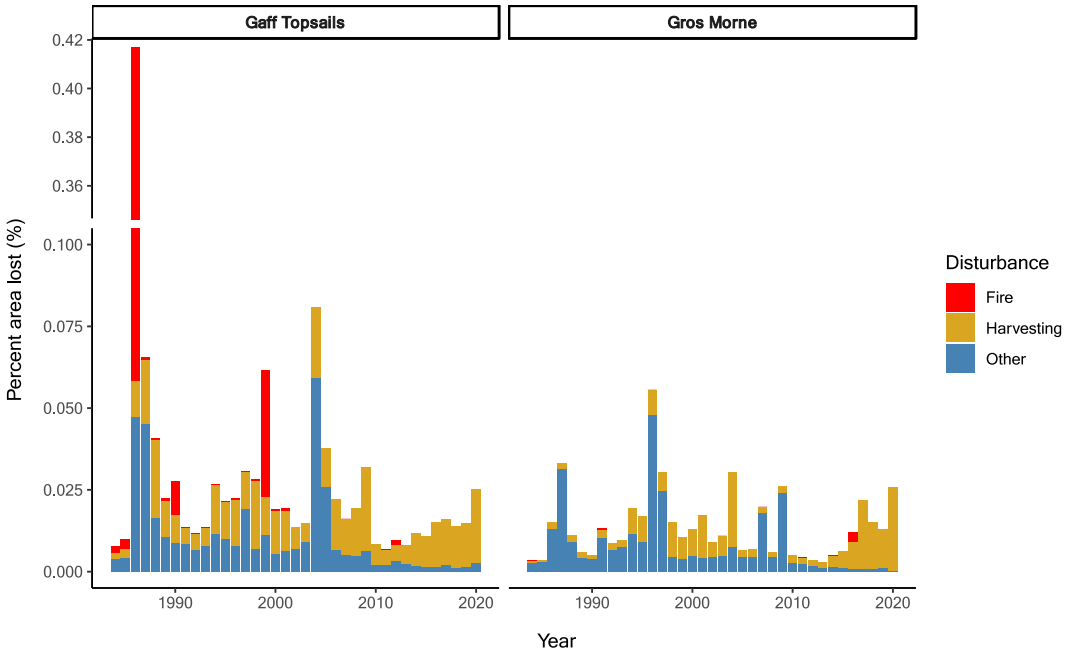

Fig. 7. Stacked bar chart showing the annual percentage of each herd region's area where lichen volume loss was directly associated with mapped disturbances, for the Gaff Topsails (left) and Gros Morne (right) herd ranges. Percentages are calculated relative to the total number of pixels within each herd range. Colors correspond to disturbance categories: fire (red), harvesting (goldenrod), and other (blue), consistent with the classification used in Fig. 6. Values are calculated only for pixels that exhibited net loss between the first (1984–1988) and last (2018–2022) periods of the time series.

volume. By providing continuous spatial estimates of lichen volume—a proxy for winter forage abundance—this work fills a key data gap for caribou habitat assessment and supports evidence-based conservation planning.

Model selection

The use of separate models for each vegetation class—coniferous forests, wetlands, and open lands—allowed us to capture distinct relationships between spectral predictors and lichen volume (Fig. 3). In open lands, predicted lichen volume followed a non-linear relationship with NDWI, driven by an interaction with vegetation type. This pattern likely reflects the moisture preferences and substrate characteristics of the two vegetation types: barrens tend to be drier and rockier, offering limited substrate for lichen colonization, while shrublands provide more favorable conditions at intermediate moisture levels. At higher moisture levels, however, lichen volume declines, consistent with reduced surface stability, greater vascular-plant competition, and diminished light availability.

Predicted lichen volume increased approximately linearly with green reflectance in both wetlands and coniferous forests (Fig. 3). Although many terrestrial lichens, such as *Cladonia alpestris*, appear green and exhibit albedo values similar to low vegetation (Petzold & Rencz, 1975), their spectral reflectance differ fundamentally from vascular plants. Lichens typically show higher reflectance across the visible spectrum, a relatively flat response in the green band, and a gradual increase from red to near-infrared wavelengths, lacking the pronounced chlorophyll-driven peak characteristic of vascular vegetation (Käyhkö & Pellikka, 1994; Nordberg & Allard, 2002; Petzold & Goward, 1988; Rees et al., 2004). This subdued green peak can be attributable to biochemical compounds such as usnic acid, a pale-yellow pigment common in several Cladonia species, whose surface crystals increase visible-wavelength reflectance and contributes to distinctive UV–blue absorption features (Ager & Milton, 1987; Petzold & Goward, 1988; Rees et al., 2004). While the green band (Landsat TM Band 2) is more commonly used within multispectral indices, such as the Tasseled Cap transformations (Crist & Cicone, 1984; Jackson & Huete, 1991), its strong contrast between pale lichen mats and surrounding vegetation or soil likely explains its effectiveness here. Consequently, higher green reflectance values in our data may correspond to lighter surfaces, such as exposed lichen mats or sparsely vegetated ground, which provide favorable conditions for terrestrial lichen growth.

Moreover, lichen absence was predicted through moisture-sensitive spectral variables included in the zero-inflation component of each vegetation-specific model: NDWI in open lands, TCW in wetlands, and SWIR1 in coniferous forests —reflecting moisture as a key ecological constraint on terrestrial lichen establishment. Through their poikilohydric nature, lichens require periodic hydration for photosynthesis and growth, yet persistently saturated conditions or dense, moist canopies create unfavorable environments for their establishment (Nash, 2008; Gauslaa, 2014). NDWI, calculated from near-infrared and green reflectance, is sensitive to soil and surface moisture through the contrasting spectral behavior of water and vegetation (McFeeters, 1996; Wang & Qu, 2007), allowing it to distinguish excessively dry substrates from more moderately moist conditions that can support lichens (Dennison et al., 2005). TCW, combining visible, near-infrared, and shortwave-infrared reflectance (Crist & Cicone, 1984), can capture vegetation and soil moisture as well as canopy structure (Cohen & Spies, 1992; Fiorella & Ripple, 1995). Similarly, SWIR1, sensitive to canopy water content, can help identify forested sites where high canopy wetness preclude the establishment of terrestrial lichen (Hunt et al., 2013).

Spatial and temporal trends in lichen volume

Our spatial predictions indicate that terrestrial lichens are widespread across Newfoundland but generally occur at low volume, with high-density patches being relatively rare. This scarcity likely reflects environmental constraints on lichen growth across much of the region, including substrate availability, moisture regimes, and disturbance history. In the Central Newfoundland ecoregion, for example, shallow and stony podzolic soils, poor drainage, and irregular terrain restrict suitable substrate for lichen establishment, while extensive peatlands further limit dry microsites (Woodrow & Heringa, 1987). In contrast, at higher elevations in the Long Range Barrens—where both study herds

occur—thin soils, strong winds, cool temperatures, and widespread heath- and moss-dominated barrens also limit lichen productivity and promote patchy cover (Woodrow & Heringa, 1987). Together, these factors help explain the predominance of low lichen volumes across the study area.

Temporal trends differed among vegetation types (Fig. 4). Wetlands and open lands (barrens and shrublands) showed little long-term change, and low or near-zero volumes were common in open lands, despite these habitat types typically supporting lichen communities. This pattern underscores lichens' sensitivity to habitat alteration and their exceptionally slow recovery, which can require decades to centuries after disturbance (Jandt et al., 2008; McMullin et al., 2013). Coniferous forests, however, exhibited more dynamic trends, with a decline in the late 1980 s, followed by a sustained increase in volume (Fig. 4). Similar expansions of lichen-dominated areas have been reported in Quebec's boreal forests following stand-replacing disturbance (Girard et al., 2007), suggesting that comparable processes may also occur in Newfoundland, although broader confirmation is needed.

At the landscape scale, total lichen volume per unit area has generally increased over time, particularly in Gros Morne (Fig. 5). This region showed a marked recovery after the early 1990s, whereas Gaff Topsails experienced a slower, more gradual increase. These differences likely reflect contrasting disturbance regimes. Much of the Gros Morne herd range lies within the large protected area that is Gros Morne National Park, where harvesting is absent and other anthropogenic or non-stand replacing disturbances are minimal. The lack of recent large-scale disturbances may have enabled lichen communities in this region to recover more rapidly and maintain higher volumes over time compared to the Gaff Topsails, where industrial activities and habitat alterations have been more prevalent. This interpretation is consistent with spatial disturbance patterns, as most harvesting occurred outside the park boundary (Fig. 6b).

Relationship between disturbance and lichen loss

The contrasting recovery trajectories between Gros Morne and the Gaff Topsails (Fig. 5) can be further interpreted through their disturbance histories (Figs. 6 and 7). Despite covering a larger area, Gaff Topsails contains a greater proportion of disturbed land, indicating higher disturbance pressure than Gros Morne. Disturbances in Gaff Topsails are more spatially widespread, and the 1986 fire—although limited in extent—was a major stand-replacing event that likely caused substantial local reductions in lichen volume. Such large disturbances, including both fire and harvesting, can have persistent effects on lichen communities, as recovery often spans decades even after recolonization begins (Jandt et al., 2008; Sirois & Payette, 1989). In Gros Morne, disturbances were generally small and confined to areas outside the park interior, resulting in limited effects on lichen communities. Given their limited extent, these disturbances may remove only small patches or create microhabitats favorable for recolonization, allowing lichen volume to remain stable or increase over time (McMullin et al., 2019). By contrast, the broader extent and intensity of disturbance in Gaff Topsails—particularly the 1986 fire and subsequent harvesting—appear to have constrained lichen recovery in that region (Fig. 7).

Implications for caribou conservation

The regional contrasts we observed, together with the limited extent of high-volume lichen patches, have important implications for boreal caribou, which rely heavily on terrestrial lichens during winter. The biomass level of ~3000 kg·ha^{-1}, reported in several studies as characteristic of stands that caribou preferentially select during winter (Joly et al., 2010; Silva et al., 2019), provides a useful benchmark for interpreting our results. Our 2022 predictions indicate that most (over 95%) of the landscape supports lichen volumes that translate to biomass levels below this benchmark, suggesting that preferred winter foraging patches are relatively limited, spatially isolated, and concentrated primarily in mature coniferous stands. The ability of our models to identify these preferred winter foraging patches is therefore critical, as conserving them will be essential for maintaining adequate winter habitat and supporting ongoing caribou recovery efforts.

Limitations

A key limitation of this study is the absence of an independent validation dataset. Although a conventional approach would be to reserve 20% of field plots for validation, this was not feasible given our limited sample size and the need to fit separate models for each vegetation type. Several classes contained few field sites (e.g., four barren land plots, nine mixed wood plots), and withholding even a small fraction would have left insufficient data to estimate model parameters reliably. Using the full dataset preserved the ecological and spectral variability necessary for stable model calibration, but it also means that predictive performance beyond the sampled sites remains uncertain.

Transferability represents another limitation. While predicted lichen volumes were reliable within our study area, caution is warranted when applying the models elsewhere, as differences in vegetation composition, lichen mat height, and ground cover can alter spectral–lichen relationships. Future work should therefore prioritize independent field validation and evaluate how predicted lichen volumes relate to caribou habitat selection and movement patterns. Since caribou tend to select areas with greater lichen availability (Joly et al., 2010; Rickbeil et al., 2017b), testing this relationship would provide an ecologically meaningful form of indirect validation of the models and help identify the patches most critical for conservation.

5. Conclusion

This study provides the first spatially explicit estimates of ground-lichen volume in Newfoundland and demonstrates the effectiveness of a habitat-stratified modeling approach for capturing spatial and temporal variability in lichen availability. By producing spatially explicit maps spanning nearly four decades, our work provides a foundational understanding of the spatial and temporal variability of lichen volume across Newfoundland and identifies where higher-volume patches tend to occur. The resulting maps offer practical value for conservation planning by highlighting areas where preferred winter foraging conditions are most likely to be sustained. Although additional validation will be required to refine predictive accuracy and assess transferability beyond the sampled sites, the framework developed here provides a foundation for linking lichen dynamics with caribou habitat selection, tracking ecological change, and guiding conservation planning within Newfoundland.

CRediT authorship contribution statement

Catherine Beaulieu: Writing – review & editing, Writing – original draft, Visualization, Methodology, Formal analysis, Data curation, Conceptualization. **Nicholas C. Coops:** Writing – review & editing, Methodology, Funding acquisition, Conceptualization. **Alexandre Morin-Bernard:** Writing – review & editing. **Steeve D. Côté:** Writing – review & editing, Supervision. **Alexis Achim:** Writing – review & editing, Supervision, Project administration, Funding acquisition, Conceptualization.

Declaration of competing interest

The authors declare that they have no known competing financial interests or personal relationships that could have appeared to influence the work reported in this paper.

Acknowledgements

This work was conducted within the framework of the Silva21 research project (NSERC ALLRP 556265–20, grantee Prof. Alexis Achim) with additional financial support from the Canadian Space Agency (22IUCLAV14, grantee Prof. Alexis Achim). We gratefully acknowledge Natural Resources Canada (NRCan), especially our collaborator Douglas Piercey (Natural Resources Canada, Atlantic Forestry Centre), for sharing boreal caribou GPS collar data and assisting with data collection. We thank the government, institutional, and industrial partners involved in Silva21 for their support, especially Kruger, whose initiative helped launch this project. We also sincerely thank the field team for their contribution to data collection, including Florence Leduc, Philippe Riel, and Benjamin Bouthenet, under the leadership of Catherine Chagnon. We additionally thank Catherine Chagnon for her support in developing the generalized linear models used in this study.

Appendix A. . Summary of field sampling sites

.

Table A1
Number of sampled field sites by vegetation type and study region. Each site corresponds to one 500 m^2 plot.

Vegetation Type	Number of sites	
	Gros Morne	Gaff Topsails
Barren Land	1	3
Shrubs	6	5
Wetland	11	16
Coniferous	8	7
Mixed Wood	5	4
Total	**31**	**35**

Appendix B. . Field sampling plot design

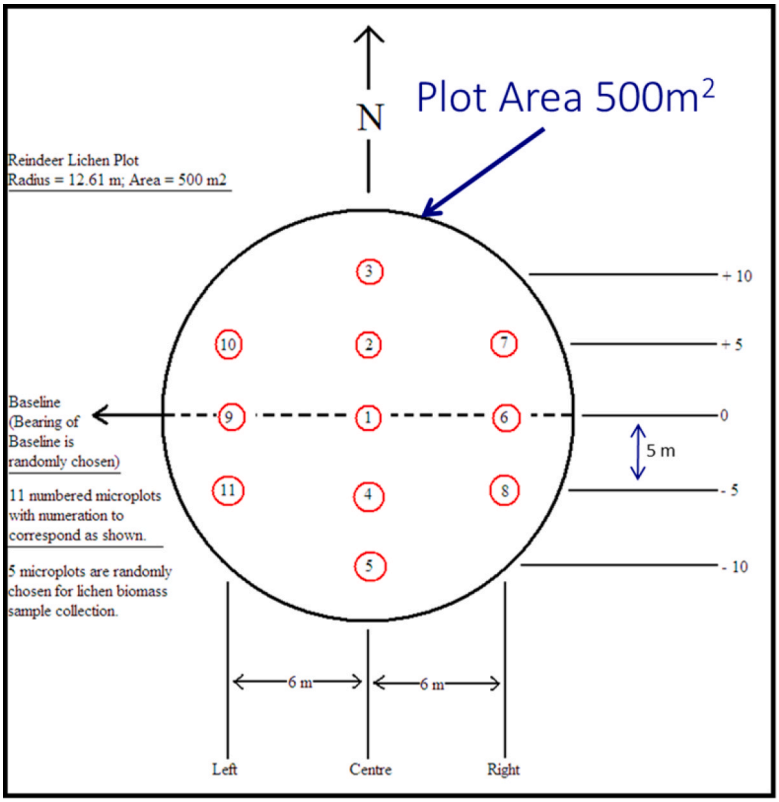

Fig. B1. Configuration of the 11 lichen microplots within the 500 m^2 circular sampling plot used in field surveys.

Appendix C. . Exploratory scatterplots and correlation plots

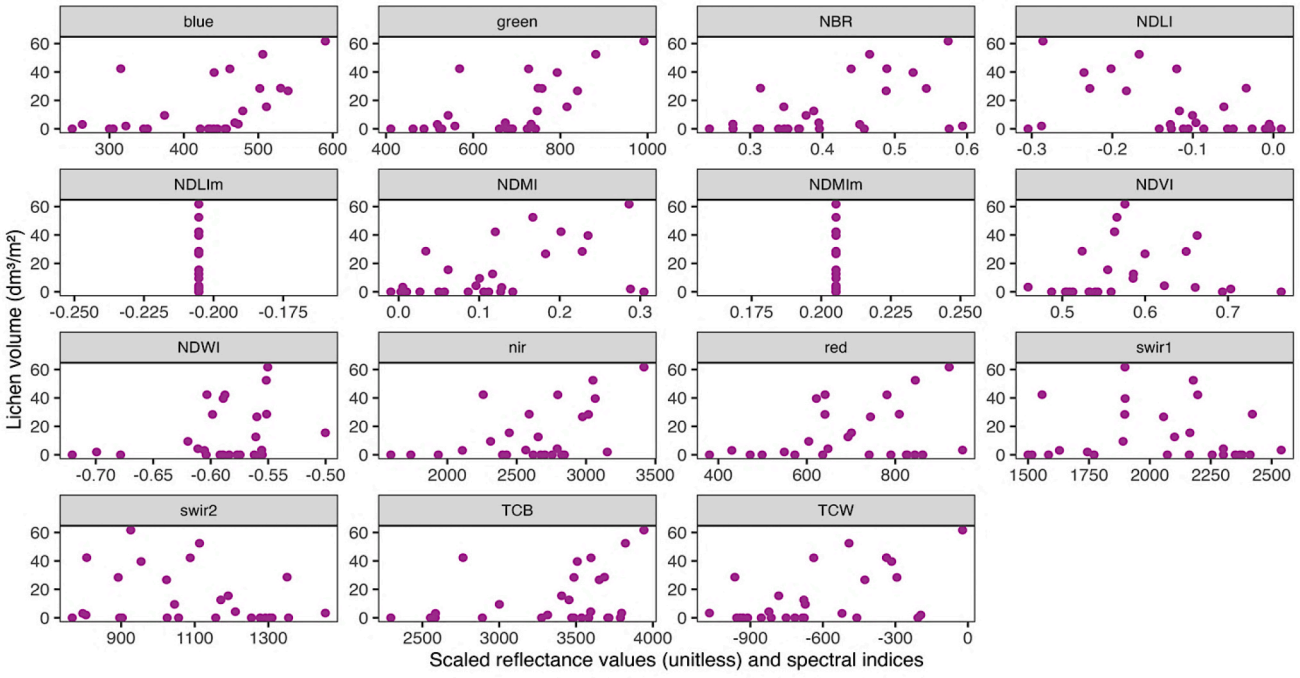

Fig. C.1. Exploratory scatterplots showing the relationship between observed lichen volume and candidate spectral predictors (scaled reflectance values of bands and vegetation indices) for wetland sites. These plots informed the visual screening of predictors used in model selection. Note: The abbreviations used in include spectral bands (blue, green, red, nir, swir1, swir2) and indices: NBR (Normalized Burn Ratio), NDLI (Normalized Difference Lichen Index), NDMI (Normalized Difference Moisture Index), NDMIm and NDLIm (global mean values of NDMI and NDLI), NDVI (Normalized Difference Vegetation Index), NDWI (Normalized Difference Water Index), (Normalized Burn Ratio), TCB (Tasseled Cap Brightness), and TCW (Tasseled Cap Wetness).

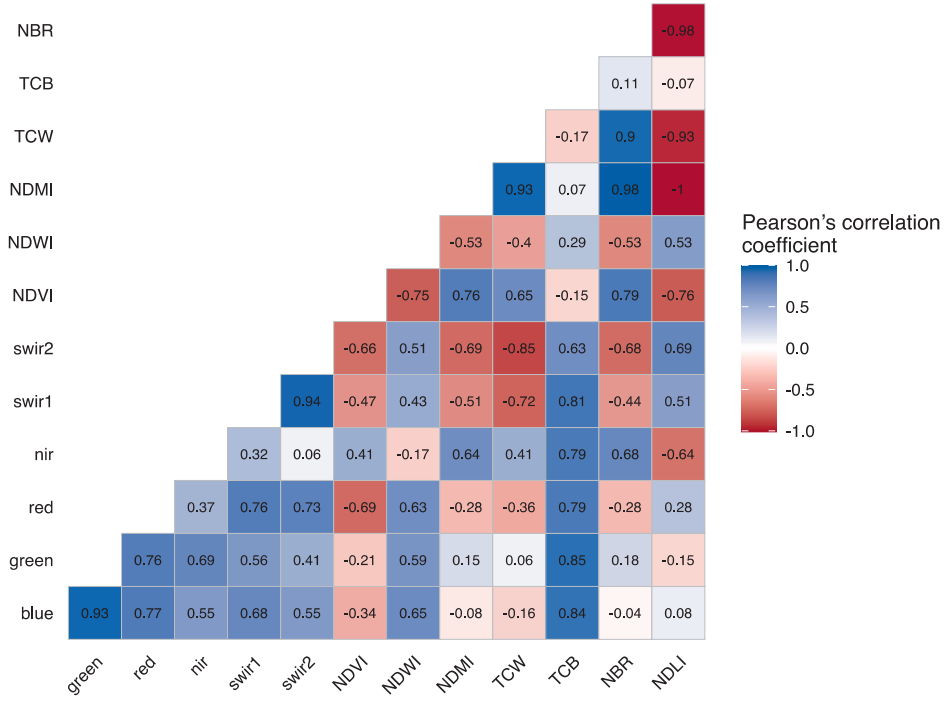

Fig. C.2. Pearson correlation matrix for candidate spectral predictors within wetland field sites, used to assess pairwise correlations and avoid collinearity in model selection. See for abbreviation definitions.

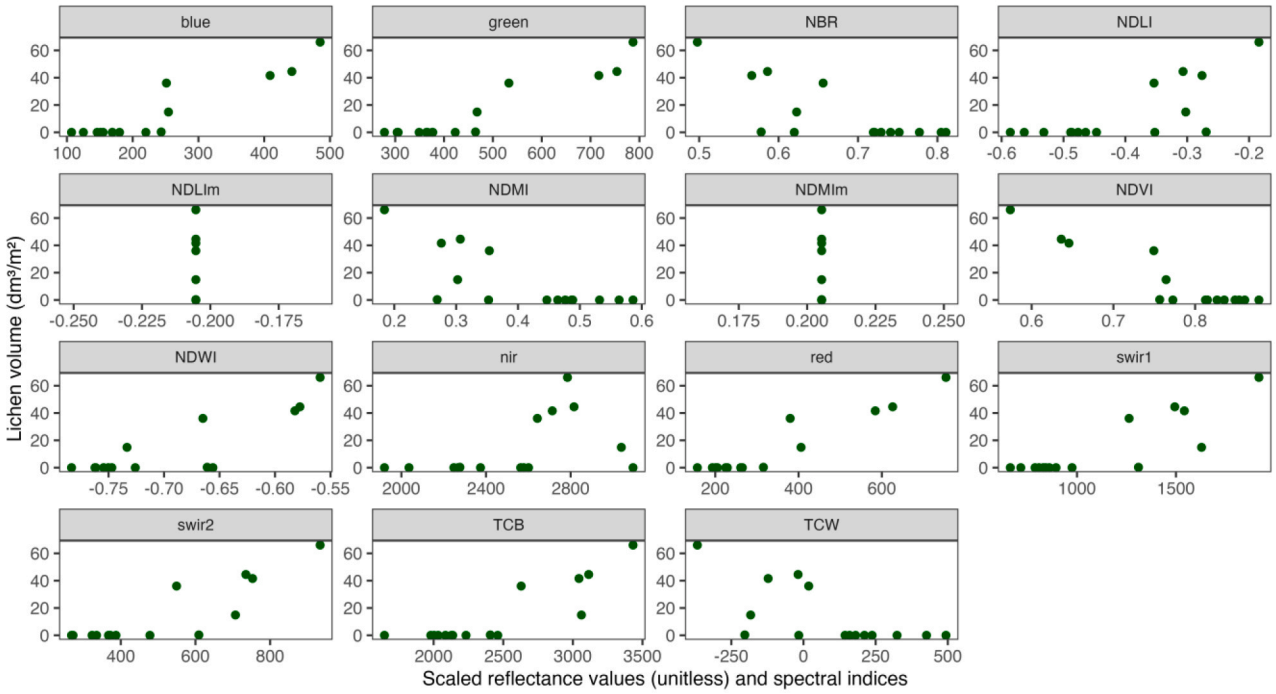

Fig. C.3. Exploratory scatterplots showing the relationship between observed lichen volume and candidate spectral predictors (scaled reflectance values of bands and vegetation indices) for coniferous sites. These plots informed the visual screening of predictors used in model selection. See for abbreviation definitions.

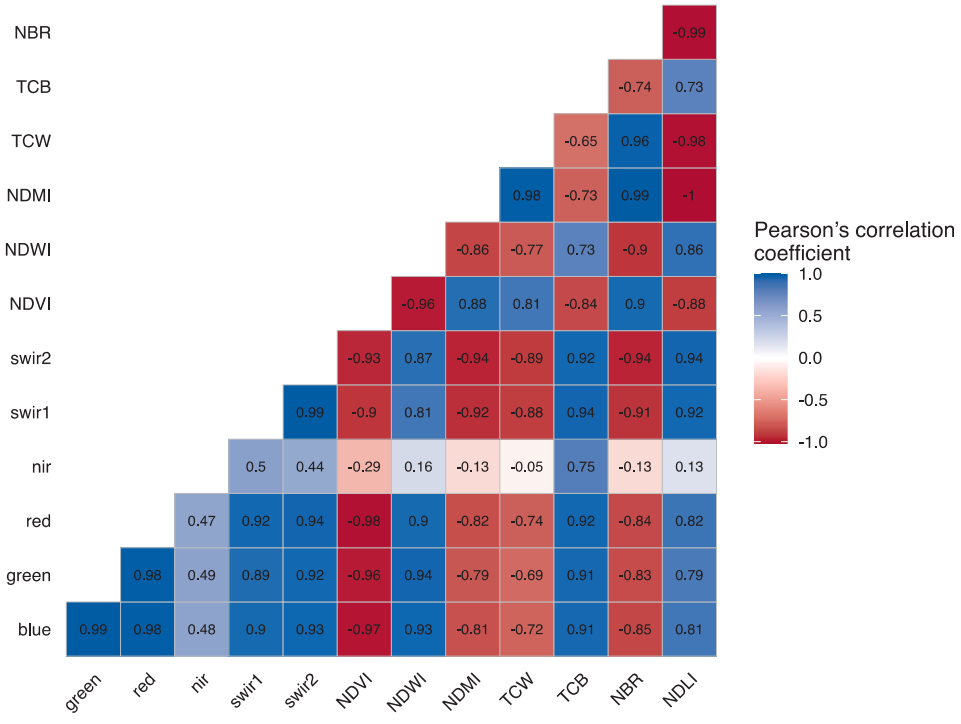

Fig. C.4. Pearson correlation matrix for candidate spectral predictors within coniferous field sites, used to assess pairwise correlations and avoid collinearity in model selection. See for abbreviation definitions.

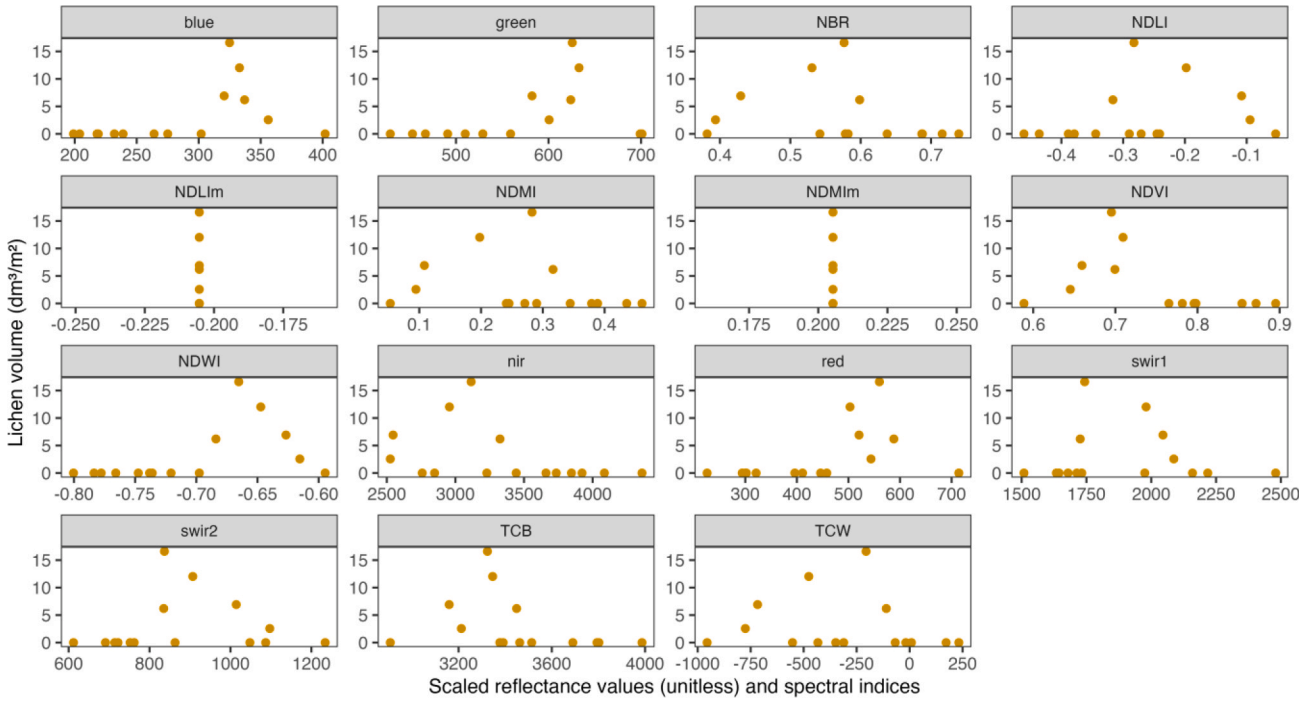

Fig. C.5. Exploratory scatterplots showing the relationship between observed lichen volume and candidate spectral predictors (scaled reflectance values of bands and vegetation indices) for open land sites (shrubland and barren land). These plots informed the visual screening of predictors used in model selection. See for abbreviation definitions.

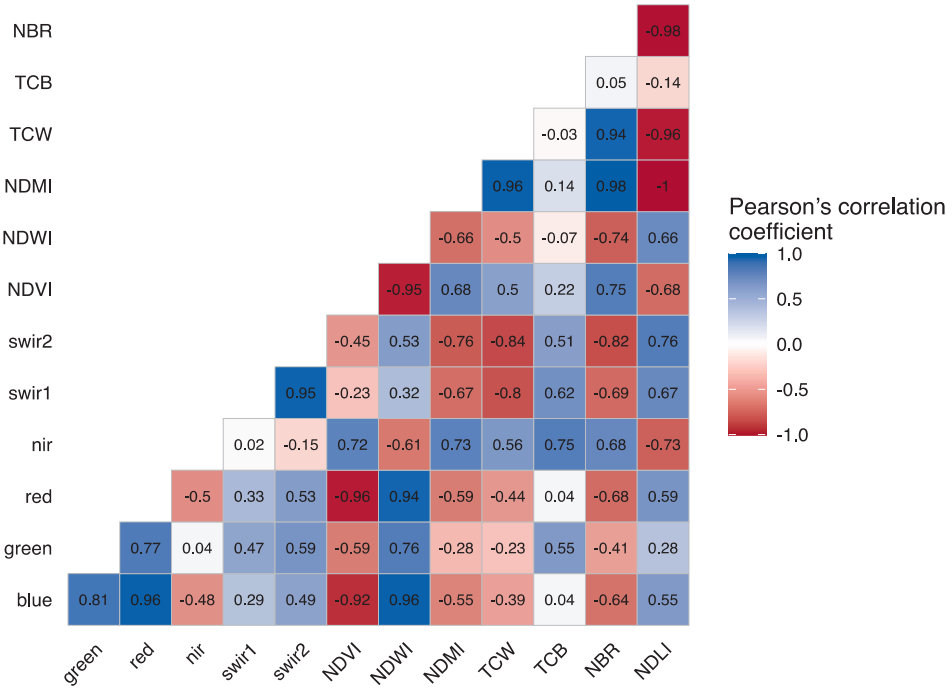

Fig. C.6. Pearson correlation matrix for candidate spectral predictors within open land field sites (shrubland and barren land), used to assess pairwise correlations and avoid collinearity in model selection. See for abbreviation definitions.

Appendix D. . Spectral predictors used in model development

Variable	Full name	Formula	Reference	Description
Blue	Blue band reflectance	–	–	Surface reflectance
Green	Green band reflectance	–	–	Surface reflectance
Red	Red band reflectance	–	–	Surface reflectance
NIR	Near infrared band reflectance	–	–	Surface reflectance
SWIR1	Shortwave Infrared Band 1 reflectance	–	–	Surface reflectance
NDVI	Normalized Difference Vegetation Index	(NIR − Red) / (NIR + Red)	Rouse et al., 1974	Vegetation productivity/ greenness
NDWI	Normalized Difference Water Index	(Green − NIR) / (Green + NIR)	McFeeters, 1996	Vegetation moisture
NBR	Normalized Burn Ratio	(NIR − SWIR2)/(NIR + SWIR2)	Key & Benson, 2006	Disturbance/burn severity/ dryness
TCB	Tasseled Cap Brightness	0.3029* Blue + 0.2786* Green + 0.4733* Red + 0.5599* NIR − 0.508* SWIR1 − 0.1872* SWIR2	Baig et al., 2014	Soil/brightness
TCW	Tasseled Cap Wetness	0.1509* Blue + 0.1973* Green + 0.3279* Red + 0.3406* NIR − 0.7112* SWIR1 − 0.4572* SWIR2	Crist & Cicone, 1984	Vegetation moisture

Appendix E. . Spatial outputs of the lichen volume models

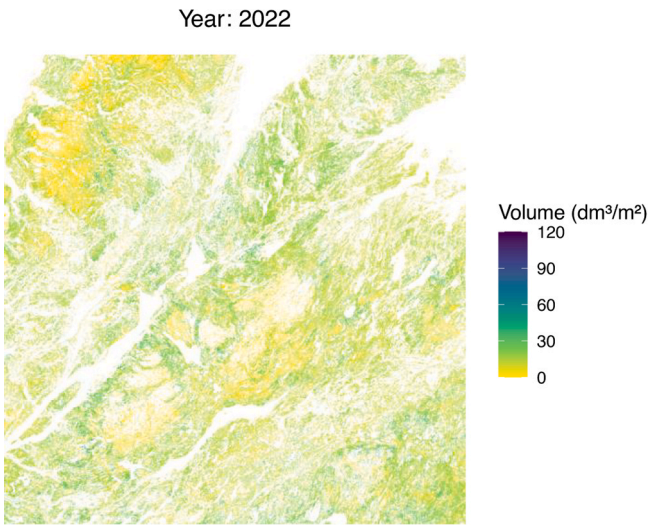

Fig. E.1. Predicted spatial distribution of lichen volume ($dm^3\ m^{-2}$) for the final year of the time series (2022) within the study area. The map illustrates the output of the vegetation-stratified modeling framework, showing spatially explicit estimates of lichen volume across heterogeneous habitat types in Newfoundland.

Data availability

The field plot dataset and R scripts used for model development, spatial prediction, and time-series analysis are available in Zenodo: https://doi.org/10.5281/zenodo.19153577. Details on access to the Landsat products and other external spatial inputs used in the workflow are provided in the repository README.

References

Adams, L.G., 2005. Effects of maternal characteristics and climatic variation on birth masses of Alaskan caribou. J. Mammal. 86, 506–513.
Ager, C.M., Milton, N.M., 1987. Spectral reflectance of lichens and their effects on the reflectance of rock substrates. Geophysics 52, 898–906.
Anderson, M., McLellan, B.N., Serrouya, R., 2018. Moose response to high-elevation forestry: implications for apparent competition with endangered caribou. J. Wildl. Manag. 82, 299–309.
Arsenault, A., LeBlanc, R., Earle, E., Brooks, D., Clarke, B., Lavigne, D., Royer, L., 2016. Unravelling the past to manage Newfoundland's forests for the future. For. Chron. 92, 487–502.
Arseneault, D., Villeneuve, N., Boismenu, C., Leblanc, Y., Deshaye, J., 1997. Estimating lichen biomass and caribou grazing on the wintering grounds of northern Quebec: an application of fire history and Landsat data. J. Appl. Ecol. 34, 65–78.
Baig, M.H.A., Zhang, L., Shuai, T., Tong, Q., 2014. Derivation of a tasselled cap transformation based on Landsat 8 at-satellite reflectance. Remote Sens. Lett. 5, 423–431.
Bergerud, A.T., 1972. Food habits of Newfoundland caribou. J. Wildl. Manag. 36, 913–923.
Boucher, Y., Arseneault, D., Sirois, L., Blais, L., 2009. Logging pattern and landscape changes over the last century at the boreal and deciduous forest transition in Eastern Canada. Landsc. Ecol. 24, 171–184.
Brooks, M.E., Kristensen, K., van Benthem, K.J., Magnusson, A., Berg, C.W., Nielsen, A., Skaug, H.J., Maechler, M., Bolker, B.M., 2017. glmmTMB balances speed and flexibility among packages for zero-inflated generalized linear mixed modeling. R J. 9, 378–400.
Crist, E.P., Cicone, R.C., 1984. A physically-based transformation of thematic mapper data—The TM Tasseled Cap. IEEE Trans. Geosci. Remote Sens. GE-22, 256–263.
Christopherson, V., Tremblay, J.-P., Gagné, P.N., Bérubé, J., St-Laurent, M.-H., 2019. Meeting caribou in the alpine: do moose compete with caribou for food? Global Ecol. Conserv. 20, e00733.
Cichowski, D., Sutherland, G.D., McNay, R.S., Sulyma, R., 2022. Direct and indirect effects of habitat disturbances on caribou terrestrial forage lichens in Montane Forests of British Columbia. Forests 13, 251.
Cohen, W.B., Spies, T.A., 1992. Estimating structural attributes of Douglas-fir/western hemlock forest stands from Landsat and SPOT imagery. Remote Sens. Environ. 41, 1–17.
COSEWIC, 2014. COSEWIC assessment and status report on the caribou (*Rangifer tarandus*), Newfoundland population, Atlantic-Gaspésie population and Boreal population, in Canada. Committee on the Status of Endangered Wildlife in Canada. Ottawa, ON.

Courtois, R., Gingras, A., Fortin, D., Sebbane, A., Rochette, B., Breton, L., 2008. Demographic and behavioural response of woodland caribou to forest harvesting. Can. J. For. Res. 38, 2837–2849.
Courtois, R., Ouellet, J.-P., Dussault, C., Gingras, A., 2004. Forest management guidelines for forest-dwelling caribou in Quebec. For. Chron. 80, 598–607.
Damman, A.W., 1983. An ecological subdivision of the island of Newfoundland. Biogeogr. Ecol. Island Newfound. 48, 163–206.
Dennison, P.E., Roberts, D.A., Peterson, S.H., Rechel, J., 2005. Use of normalized difference water index for monitoring live fuel moisture. Int. J. Remote Sens. 26, 1035–1042.
Edmonds, E. J., Bloomfield, M., 1984. *A study of woodland caribou (Rangifer tarandus caribou) in west central Alberta, 1979-1983*. Alberta Energy and Natural Resources, Fish and Wildlife Division, Edmonton, AB.
Environment Canada, 2011. Scientific Assessment to Inform the Identification of Critical Habitat for Woodland Caribou (Rangifer tarandus caribou), Boreal Population, in Canada: 2011 update. Environment Canada, Ottawa, ON.
Environment and Climate Change Canada, 2020. *Amended Recovery Strategy for the Woodland Caribou (Rangifer tarandus caribou), Boreal Population, in Canada*. Species at Risk Act Recovery Strategy Series. Environment and Climate Change Canada, Ottawa, ON.
Falldorf, T., Strand, O., Panzacchi, M., Tømmervik, H., 2014. Estimating lichen volume and reindeer winter pasture quality from Landsat imagery. Remote Sens. Environ. 140, 573–579.
Festa-Bianchet, M., Ray, J.C., Boutin, S., Côté, S.D., Gunn, A., 2011. Conservation of caribou (Rangifer tarandus) in Canada: an uncertain future. Can. J. Zool. 89, 419–434.
Fiorella, M., Ripple, W.J., 1995. Analysis of conifer forest regeneration using Landsat Thematic Mapper data. Photogramm. Eng. Remote Sens. 59, 1383–1388.
Fisheries, Forestry and Agriculture, 2021. *Caribou Conservation and Management. 2021-2022 Hunting and Trapping Guide*. https://www.gov.nl.ca/hunting-trapping-guide/2021-22/labrador-caribou/.
Fraser, R.H., Pouliot, D., van der Sluijs, J., 2022. UAV and high resolution satellite mapping of Forage Lichen (Cladonia spp.) in a Rocky Canadian Shield Landscape. Can. J. Remote. Sens. 48, 5–18.
Gauslaa, Y., 2014. Rain, dew, and humid air as drivers of morphology, function and spatial distribution in epiphytic lichens. Lichenologist 46, 1–16.
Girard, F., Payette, S., Gagnon, R., 2007. Rapid expansion of lichen woodlands within the closed-crown boreal forest zone over the last 50 years caused by stand disturbances in eastern Canada. J. Biogeogr. 35, 529–537.
Greuel, R.J., Degré-Timmons, G.É., Baltzer, J.L., Johnstone, J.F., McIntire, E.J.B., Day, N. J., Hart, S.J., McLoughlin, P.D., Schmiegelow, F.K.A., Turetsky, M.R., Truchon-Savard, A., van Telgen, M.D., Cumming, S.G., 2021. Predicting patterns of terrestrial lichen biomass recovery following boreal wildfires. Ecosphere 12, e03481.
Hartig, F., 2024. *DHARMa: residual diagnostics for hierarchical (multi-level/mixed) regression models* (R package version 0.4.7). https://CRAN.R-project.org/package=DHARMa.
He, L., Chen, W., Leblanc, S.G., Lovitt, J., Arsenault, A., Schmelzer, I., Fraser, R.H., Latifovic, R., Sun, L., Prévost, C., 2021. Integration of multi-scale remote sensing data for reindeer lichen fractional cover mapping in Eastern Canada. Remote Sens. Environ. 267, 112731.
Hermosilla, T., Wulder, M.A., White, J.C., Coops, N.C., Hobart, G.W., 2015. Regional detection, characterization, and attribution of annual forest change from 1984 to 2012 using Landsat-derived time-series metrics. Remote Sens. Environ. 170, 121–132.
Hermosilla, T., Wulder, M.A., White, J.C., Coops, N.C., Hobart, G.W., 2018. Disturbance-informed annual land cover classification maps of Canada's forested ecosystems for a 29-year landsat time series. Can. J. Remote. Sens. 44, 67–87.
Hermosilla, T., Wulder, M.A., White, J.C., Coops, N.C., 2022. Land cover classification in an era of big and open data: Optimizing localized implementation and training data selection to improve mapping outcomes. Remote Sens. Environ. 268, 112780.
Hermosilla, T., Wulder, M.A., White, J.C., Coops, N.C., Hobart, G.W., Campbell, L.B., 2016. Mass data processing of time series Landsat imagery: Pixels to data products for forest monitoring. Int. J. Digit. Earth 9, 1035–1054.
Hunt Jr., E.R., Ustin, S.L., Riano, D., 2013. Remote sensing of leaf, canopy, and vegetation water contents for satellite environmental data records. In: Qu, J., Powell, A., Sivakumar, M. (Eds.), *Satellite-Based Applications on Climate Change*. Springer, pp. 335–357.
Jackson, R.D., Huete, A.R., 1991. Interpreting vegetation indices. Prev. Vet. Med. 11, 185–200.
Jandt, R., Joly, K., Randy Meyers, C., Racine, C., 2008. Slow recovery of lichen on burned caribou winter range in Alaska tundra: potential influences of climate warming and other disturbance factors. Arct. Antarct. Alp. Res. 40, 89–95.
Johnson, C.J., Parker, K.L., Heard, D.C., 2001. Foraging across a variable landscape: Behavioral decisions made by woodland caribou at multiple spatial scales. Oecologia 127, 590–602.
Joly, K., Chapin III, F.S., Klein, D.R., 2010. Winter habitat selection by caribou in relation to lichen abundance, wildfires, grazing, and landscape characteristics in northwest Alaska. Ecosci. 17, 321–333.
Käyhkö, J., Pellikka, P., 1994. Remote sensing of the impact of reindeer grazing on vegetation in northern Fennoscandia using SPOT XS data. Polar Res. 13, 115–124.
Key, C.H., Benson, N.C., 2006. Landscape assessment: ground measure of severity, the Composite Burn Index; and remote sensing of severity, the Normalized Burn Ratio (General Technical Report RMRS-GTR-164-CD). USDA Forest Service, Rocky Mountain Research Station, Ogden, UT.
Kuusinen, N., Juola, J., Karki, B., Stenroos, S., Rautiainen, M., 2020. A spectral analysis of common boreal ground lichen species. Remote Sens. Environ. 247, 111955.
Macander, M.J., Palm, E.C., Frost, G.V., Herriges, J.D., Nelson, P.R., Roland, C., Russell, K.L.M., Suitor, M.J., Bentzen, T.W., Joly, K., Goetz, S.J., Hebblewhite, M., 2020. Lichen cover mapping for caribou ranges in interior Alaska and Yukon. Environ. Res. Lett. 15, 055001.
Mahoney, S.P., Lewis, K.P., Weir, J.N., Morrison, S.F., Luther, J.G., Schaefer, J.A., Pouliot, D., Latifovic, R., 2016. Woodland caribou calf mortality in Newfoundland: insights into the role of climate, predation and population density over three decades of study. Popul. Ecol. 58, 91–103.
Mahoney, S.P., Virgl, J.A., 2003. Habitat selection and demography of a nonmigratory woodland caribou population in Newfoundland. Can. J. Zool. 81, 321–334.
Manson, K.K., McDermott, J.P., Powell, L.L., Whitaker, D.M., Warkentin, I.G., 2020. Assessment of Rusty Blackbird habitat occupancy in the Long Range Mountains of Newfoundland, Canada using forest inventory data. Diversity 12, 340.
Matasci, G., Hermosilla, T., Wulder, M.A., White, J.C., Coops, N.C., Hobart, G.W., Bolton, D.K., Tompalski, P., Bater, C.W., 2018. Three decades of forest structural dynamics over Canada's forested ecosystems using Landsat time-series and lidar plots. Remote Sens. Environ. 216, 697–714.
McFeeters, S.K., 1996. The use of the Normalized Difference Water Index (NDWI) in the delineation of open water features. Int. J. Remote Sens. 17, 1425–1432.
McKenney, D.W., Pedlar, J.H., Papadopol, P., Hutchinson, M.F., 2006. The development of 1901–2000 historical monthly climate models for Canada and the United States. Agric. For. Meteorol. 138, 69–81.
McMullin, R.T., Thompson, I.D., Lacey, B.W., Newmaster, S.G., 2011. Estimating the biomass of woodland caribou forage lichens. Can. J. For. Res. 41, 1961–1969.
McMullin, R.T., Thompson, I.D., Newmaster, S.G., 2013. Lichen conservation in heavily managed boreal forests. Conserv. Biol. 27, 1020–1030.
McMullin, R.T., Wiersma, Y.F., Newmaster, S.G., Lendemer, J.C., 2019. Risk assessment and conservation strategies for rare lichen species and communities threatened by sea-level rise in the Mid-Atlantic Coastal Plain. Biol. Conserv. 239, 108281.
Meades, W.G., 2008. Vegetation of newfoundland. In: S.S. Talbot (Ed.) Proceedings of the Fourth International Conservation of Arctic Flora and Fauna (CAFF) Flora Group Workshop, 15–18 May 2007, Tórshavn, Faroe Islands, pp. 16–20. CAFF Technical Report No. 15. CAFF, Akureyri, Iceland.
Meades, W., Roberts, B., 1992. A review of forest site classification activities in Newfoundland and Labrador. For. Chron. 68, 25–33.
Nash, T.H., 2008. *Lichen Biology* (2nd ed). Cambridge University Press.
Nelson, P.R., Roland, C., Macander, M.J., McCune, B., 2013. Detecting continuous lichen abundance for mapping winter caribou forage at landscape spatial scales. Remote Sens. Environ. 137, 43–54.
Nordberg, M.-L., 1998. Vegetation and biomass changes in mountainous areas in sweden using satellite and airborne imaging scanner data. In: Proceedings of the IEEE International Geoscience and Remote Sensing Symposium (IGARSS '98): Information for Sustainability, vol. 1. Information for Sustainability, pp. 431–435.
Nordberg, M.L., Allard, A., 2002. A remote sensing methodology for monitoring lichen cover. Can. J. Remote. Sens. 28, 262–274.
O'Brien, D., Manseau, M., Fall, A., Fortin, M.-J., 2006. Testing the importance of spatial configuration of winter habitat for woodland caribou: an application of graph theory. Biol. Conserv. 130, 70–83.
Parker, K.L., Barboza, P.S., Stephenson, T.R., 2005. Protein conservation in female caribou (Rangifer tarandus): effects of decreasing diet quality during winter. J. Mammal. 86, 610–622.
Petzold, D.E., Goward, S.N., 1988. Reflectance spectra of subarctic lichens. Remote Sens. Environ. 24, 481–492.
Petzold, D.E., Rencz, A.N., 1975. The albedo of selected subarctic surfaces. Arct. Alp. Res. 7, 393–398.
R Core Team, 2024. *R: A Language and Environment for Statistical Computing* [software]. R Foundation for Statistical Computing, https://www.R-project.org/.
Rees, W., Tutubalina, O., Golubeva, E., 2004. Reflectance spectra of subarctic lichens between 400 and 2400 nm. Remote Sens. Environ. 90, 281–292.
Rickbeil, G.J., Hermosilla, T., Coops, N.C., White, J.C., Wulder, M.A., 2017a. Barren-ground caribou (Rangifer tarandus groenlandicus) behaviour after recent fire events; integrating caribou telemetry data with Landsat fire detection techniques. Glob. Chang. Biol. 23, 1036–1047.
Rickbeil, G.J., Hermosilla, T., Coops, N.C., White, J.C., Wulder, M.A., 2017b. Estimating changes in lichen mat volume through time and related effects on barren ground caribou (Rangifer tarandus groenlandicus) movement. PLoS One 12, e0172669.
Rouse, J. W., Haas, R. H., Schell, J. A., Deering, D. W., 1974. Monitoring vegetation systems in the Great Plains with ERTS. In *Third Earth Resources Technology Satellite-1 Symposium* (NASA SP-351).
Ruppert, J.L.W., Fortin, M.-J., Gunn, E.A., Martell, D.L., 2016. Conserving woodland caribou habitat while maintaining timber yield: a graph theory approach. Can. J. For. Res. 46, 914–923.
Scotter, G. W., 1965. Study of the winter range of barren-ground caribou with special reference to the effects of forest fires (Wildlife Management Series, Progress Report No. 3). Canadian Wildlife Service, Ottawa, ON.
Silva, J.A., Nielsen, S.E., Lamb, C.T., Hague, C., Boutin, S., 2019. Modelling lichen abundance for woodland caribou in a fire-driven boreal landscape. Forests 10, 962.
Sirois, L., Payette, S., 1989. Postfire black spruce establishment in subarctic and boreal Quebec. Can. J. For. Res. 19, 1571–1580.
Théau, J., Peddle, D., Duguay, C., 2005. Mapping lichen in a caribou habitat of Northern Quebec, Canada, using an enhancement classification method and spectral mixture analysis. Remote Sens. Environ. 94, 232–243.
Väre, H., Ohtonen, R., Mikkola, K., 1996. The effect and extent of heavy grazing by reindeer in oligotrophic pine heaths in northeastern Fennoscandia. Ecography 19, 245–253.

Wang, L., Qu, J.J., 2007. NMDI: a normalized multi-band drought index for monitoring soil and vegetation moisture with satellite remote sensing. Geophys. Res. Lett. 34.
Waterhouse, M.J., Armleder, H.M., Nemec, A.F., 2011. Terrestrial lichen response to partial cutting in lodgepole pine forests on caribou winter range in west-central British Columbia. Rangifer 31, 119–134.
White, J.C., Wulder, M.A., Hermosilla, T., Coops, N.C., Hobart, G.W., 2017. A nationwide annual characterization of 25 years of forest disturbance and recovery for Canada using Landsat time series. Remote Sens. Environ. 194, 303–321.
White, J.C., Wulder, M.A., Hobart, G.W., Luther, J.E., Hermosilla, T., Griffiths, P., Coops, N.C., Hall, R.J., Hostert, P., Dyk, A., 2014. Pixel-based image compositing for large-area dense time series applications and science. Can. J. Remote. Sens. 40, 192–212.
Wilson, E.H., Sader, S.A., 2002. Detection of forest harvest type using multiple dates of Landsat TM imagery. Remote Sens. Environ. 80, 385–396.
Wittmer, H.U., McLellan, B., Serrouya, R., Apps, C.D., 2007. Changes in landscape composition influence the decline of a threatened woodland caribou population. J. Anim. Ecol. 76, 568–579.
Woodrow, E. F., Heringa, P. K., 1987. Pedoclimatic zones of the island of Newfoundland (Report No. 32). Canada Soil Survey, Agriculture Canada, St. John's, NL.